

# Friction in a Thin Water Layer: Dissociative versus Nondissociative Friction

M. Paliy,<sup>†,‡</sup> O. M. Braun,<sup>\*,§</sup> and S. Consta<sup>||</sup>

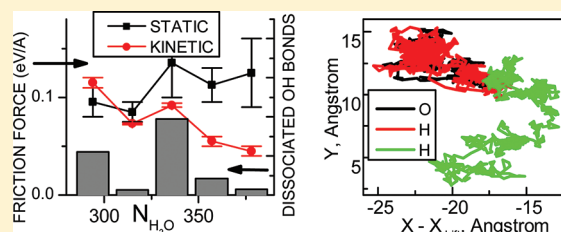
<sup>†</sup>Department of Chemistry and Surface Science Western, University of Western Ontario, London N6A 5B7, Ontario, Canada

<sup>‡</sup>Entropique Scientific Research Inc., London N6J 3S2, Ontario, Canada

<sup>§</sup>Institute of Physics, National Academy of Sciences of Ukraine, 03028 Kiev, Ukraine

<sup>||</sup>Department of Chemistry, University of Western Ontario, London N6A 5B7, Ontario, Canada

**ABSTRACT:** An ultrathin water film confined between two substrates in moving contact is studied using Langevin molecular dynamics with a coordinate- and velocity-dependent damping coefficient. The water molecules are modeled with the Central-Force model that allows for the dissociation of water molecules into  $H^+$  and  $OH^-$ . Two different friction scenarios are found depending on the applied pressure and the strength of the interaction of water with substrates. Under low loads, the water molecules stay intact during the frictional sliding. However, when the applied pressure increases past a value of  $\sim 20$  GPa, the water molecules begin to dissociate and recombine immediately in the course of sliding, which results in a large increase of friction. The rate of such dissociation is found to be roughly proportional to the speed of driving. The relation of the observed phenomena to the “superionic” and “ionic fluid” states of water and its relevance in practical friction situations is discussed.



## 1. INTRODUCTION

Water is one of the most abundant materials on Earth. In particular, water from humidity almost always contaminates contact areas between solid bodies in natural or industrial environments.<sup>1</sup> Moreover, nature selected water as a basic constituent for the biological lubricants that are far superior to the manmade oil-based lubricants.<sup>2</sup> Surprisingly, water itself did not attract, until recently, much attention as a lubricant in manmade devices, due to two reasons: first, many surfaces undergo corrosion in the presence of water, and second, the water may be squeezed out from the contact area due to its very low viscosity. However, both of these problems could be resolved by a proper choice of surfaces coated for protection against corrosion and by use of sufficiently hydrophilic surfaces to avoid squeezing out the water.

Understanding the role of water and the effect of the nature of surfaces in friction involves first of all knowledge of the phase behavior of water under confinement. Even in the bulk, the phase diagram of water is quite intricate, especially around the freezing point, where water demonstrates anomalies related to the hydrogen bonding between its molecules.<sup>3,4</sup> Its behavior can be dramatically different in a confined geometry, i.e., in a thin nanoscale layer. Both experiment<sup>5,6</sup> and computer simulation<sup>7–13</sup> of thin layers of water reveal the transitions between various liquid, amorphous, and crystalline phases of water and ice, not found in the bulk.

Several studies, both experimental ones<sup>14–16</sup> and computer simulations (see, e.g., ref 17), were devoted to the role of ions in the lubrication of various surfaces by water, illuminating the role of ions in effective lubrication and the so-called “hydration lubrication” mechanism. These, as well as other<sup>13</sup> studies,

revealed the following generic behavior of confined water: it stays fluid at least down to the thickness of a few molecular layers. Study of biologically important systems of water adsorbed at hydrophilic self-assembled monolayers<sup>18</sup> has shown an intricate interplay between water and the self-assembled layers. It also corroborated the statement that the interfacial dynamics of water remains liquid.

Our previous simulation of the frictional properties of very thin water layers (down to one or two monolayers)<sup>19</sup> has demonstrated, in accord with the above-mentioned studies, that the viscosity of water confined between two atomically flat hydrophilic surfaces is increased but still lies within a factor of 2 of its bulk value.<sup>14,15</sup> More recently, both the retaining of high diffusivity and thus low viscosity values by water and the reduction of water frictional properties by adding salt (ions) to it have been confirmed in the simulation of the thin water layers confined between carbon nanotube array surfaces.<sup>20</sup> Both these studies have found, somewhat counterintuitively, that more “hydrophilic” surfaces exhibit lower friction, compared to more “hydrophobic” ones, ultimately due to subtle differences in the geometric factors (roughness of the free-energy profiles). Another recent systematic study of water between both hydrophilic and hydrophobic surfaces demonstrated the increase of water viscosity by 2 to 4 times in the hydrophilic case, due to the surface trapping of water molecules, while water diffusivity has been found to have the same value in both cases.<sup>21,22</sup> By contrast, for decreasing strength of interaction

Received: November 8, 2011

Revised: March 10, 2012

Published: March 21, 2012

between water and its confining surfaces (i.e., for their increasing hydrophobicity), the boundary slip length has been found to increase, thus leading to the effective reduction of friction.<sup>22</sup> In the present work, we clarify the reasons why in the system we studied in ref 19 the more “hydrophobic” surfaces have elevated friction.

An important observation commonly cited in the literature<sup>1</sup> is that, in a frictional contact, water or other lubricant may be subjected to the extremely high pressures of the order of tens of GPa that correspond to the yield strengths of the common materials. This is because the area of real contact between two rough surfaces (that join each other at the microscopic asperities) is usually many orders of magnitude smaller than the apparent area of contact. At such high pressure, that is also accompanied by shear, the process of the dissociation of water may become possible. In this study, we report that such a dissociation indeed occurs immediately during frictional sliding, and we show that it leads to a strong increase of the friction force. In this regard, it is interesting to relate our findings to the pioneering studies of hot and dense water by Cavazzoni et al.<sup>23</sup> and Goldman et al.,<sup>24</sup> who modeled via ab initio molecular dynamics the exotic “superionic” and “ionic fluid” dissociated states of water found at extremely high pressures on Giant planets of the Solar System. Most recently, it has also been emphasized that similar conditions may be encountered in more earthly environments, e.g., in the shock waves, explosions, etc.<sup>25–28</sup> Equilibrium melting of ice under high pressures has been investigated in refs 29–32.<sup>29–32</sup> In particular, it has been found<sup>29</sup> that the onset of molecular dissociation of water under pressure is a gradual process, while the location of the exact regions of temperature and pressure at which the dissociation occurs is still a debatable issue. Moreover, when high pressure is accompanied by strong out-of-equilibrium frictional driving, the conditions for dissociation may strongly differ from the equilibrium ones.

## 2. MODEL

We use the Molecular Dynamics (MD) technique based on Langevin equations with coordinate- and velocity-dependent damping coefficient<sup>33,34</sup> to study a thin film of water confined between two flat substrates. Each of the substrates is made of two layers of  $N_{\text{sub}} = 24 \times 11$  atoms organized into lattices of square symmetry with the lattice constants  $a_x = a_y = 2.5 \text{ \AA}$  (to check for the absence of the substrate commensurability effects on friction,<sup>35,36</sup> we have also used the setup with bottom substrate atomic lattice rotated by some angle with respect to the top one<sup>37</sup>). The outer substrate layers are rigid, while the atoms belonging to the layers in the immediate contact with the lubricant are allowed to move in three spacial directions. The outmost layer of the bottom substrate is kept fixed, while the outmost layer of the top substrate is driven by a stage with a velocity  $v_s$  through an attached spring of elastic constant  $k_s = 10^{-3} \text{ eV/\AA}^2$  per atom. Between the substrates, we put  $N_{\text{H}_2\text{O}}$  water molecules as shown in Figure 1. In the  $x$  and  $y$  directions, we apply periodic boundary conditions.

For the interactions in water, we use the Central-Force (CF) model, originally introduced by Lemberg, Stillinger, and Rahman.<sup>38,39</sup> This model has the advantages that it is simple (pairwise interactions, no artificially introduced bond constraints) and dissociative, and with some refinements to correct the hydrostatic pressure,<sup>40</sup> it yields a quite reliable description of water.

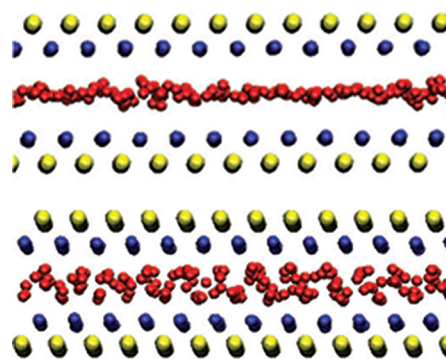


**Figure 1.** Model of the confined water film. Red spheres show the oxygen atomic sites in the water molecules (hydrogens are not shown), while yellow and blue spheres depict the atomic sites of the outer (rigid) and inner (flexible) substrate layers, respectively. The load and shear are applied to the rigid part of the top substrate. The rigid part of the bottom substrate is fixed. The top and bottom panels demonstrate two typical structures of the water lubricant film ( $N_{\text{H}_2\text{O}} = 336$ ) that correspond to different values of the load  $f_1$  and the water–substrate interaction  $V_{\text{SO}}$ . (Top) The one-layer structure observed at high loads  $f_1 \sim 1 \text{ eV/\AA}$  (the concrete value of  $f_1$  depends on the water–substrate interaction  $V_{\text{SO}}$ ). Some buckling of the layer can be observed for this kind of structure too. (Bottom) The two-layer structure (either liquid or solidified) observed at lower loads and lower values of the substrate–water interaction.

In the CF model, the pair interactions between all oxygen and hydrogen atoms have the following form

$$V_{ij}(r) = A_{ij}^{(1)}/r + A_{ij}^{(2)}/r\beta_{ij}^{(2)} + A_{ij}^{(3)}[1 + e^{\gamma_{ij}^{(3)}(r-\rho_{ij}^{(3)})}]^{-1} + A_{ij}^{(4)}[1 + e^{\gamma_{ij}^{(4)}(r-\rho_{ij}^{(4)})}]^{-1} + A_{ij}^{(5)}e^{-\delta_{ij}^{(5)}(r-\rho_{ij}^{(5)})^2} + A_{ij}^{(6)}e^{-\delta_{ij}^{(6)}(r-\rho_{ij}^{(6)})^2} \quad (1)$$

where the index  $ij$  is equal to OO, OH, or HH for the corresponding atomic pair, and the values of all coefficients in eq 1 are taken from ref 40. The long-range Coulombic part of the interaction (that corresponds to the charges  $q_{\text{H}} \approx +0.33e$ ,  $q_{\text{O}} \approx -0.66e$ ,  $e$  being the electron charge) is handled via 3D Ewald summation with  $z$ -dipole correction for the slab geometry.<sup>41</sup> The size of the system in the  $z$  direction is taken as  $L_z = 60 \text{ \AA}$ , compared to a typical slab thickness of 10–13  $\text{\AA}$  and the box sizes in the periodic directions  $L_x = 60 \text{ \AA}$  and  $L_y = 27.5 \text{ \AA}$ . We use the Ewald parameter  $r_{\text{E}} = 3.33 \text{ \AA}$ , whereas the reciprocal space sum has been cut off at a distance of  $1.13 \text{ \AA}^{-1}$ , which includes 1274 wavevectors into the summation. All short-range interactions in the model are smoothly truncated at  $r_c = 10 \text{ \AA}$ .

The substrate atoms interact with the water and between themselves via generalized Lennard-Jones (LJ) potential

$$V_{ij}(r) = [V_{ij}^{(0)}/(\mu - \nu)][\nu(r_{ij}^{(0)}/r)^\mu - \mu(r_{ij}^{(0)}/r)^\nu]$$

For the interaction between the substrate atoms (denoted as S), the parameters are  $\mu = 8$ ,  $\nu = 4$ ,  $V_{\text{SS}}^{(0)} = 1 \text{ eV}$ , and  $r_{\text{SS}}^{(0)} = 2.5 \text{ \AA}$  (this mimics approximately a quartz-like material). For the interactions between the substrate and water, we took  $\mu = 12$  and  $\nu = 6$ , and the parameters for the substrate–oxygen and substrate–hydrogen interaction are  $r_{\text{SO}} = 3.55 \text{ \AA}$ ,  $r_{\text{SH}} = 3.19 \text{ \AA}$ , and  $V_{\text{SH}} = 0.5V_{\text{SO}}$ , which describe approximately the van der Waals interaction between a water molecule and a quartz ( $\text{SiO}_2$ ) surface.<sup>8,9</sup> The value of  $V_{\text{SO}}$  was varied from zero up to

0.25 eV which is a value of the order of the hydrogen bonding interaction between water molecules. In friction studies, we mainly use two values for the water–substrate interaction: a relatively strong interaction  $V_{SO} = 0.05$  eV which we interpret as the “hydrophilic” surface and a very small interaction  $V_{SO} = 0.0025$  eV which corresponds to the “hydrophobic” surface.

The atomic masses were taken as  $m_O = 16$  amu and  $m_H = 1$  amu, and for the atoms of the substrates, the silicon atom mass  $m_S = 28.1$  amu. The equations of motions were integrated using the velocity-Verlet algorithm with the time step of 0.5 fs dictated by the CF model. The load force applied to the upper substrate was varied within the interval  $f_1 = 10^{-3}$ – $10$  eV/Å per one substrate atom, which corresponds to the pressures  $P = f_1/(a_x a_y) = 2.56 \times 10^{11}$  Pa. Note, however, that even the corrected CF model still overestimates the normal pressure of 1 bar by approximately 100 times,<sup>40</sup> so that the use of even higher pressures in simulations can be considered as a reasonable range of values.

The coordinate- and velocity-dependent damping coefficient  $\eta(z, v)$  in Langevin equations for the atomic motion has been designed to mimic a realistic situation, as described in detail in refs 33 and 34. Here we sketch only its main features: (i) the damping  $\eta(z, v) = \eta_1(z)\eta_2(v)$  exponentially decays away from the substrates as  $\eta_1(z) = 1 - \tanh[(z - a^*)/a^*]$ , where  $a^* = 3$  Å is a characteristic distance of the order of lattice spacing; (ii) its velocity dependence  $\eta_2(v) = \eta_{\min} + \eta_{\text{ph}}(\omega_{\text{wash}})$ , where  $\omega_{\text{wash}}(v) = 2\pi v/a^*$  is the washboard frequency of driving, includes a frequency-dependent phonon term  $\eta_{\text{ph}}(\omega)$  vanishing beyond a cutoff (Debye) frequency of the substrate  $\omega^* \approx 65.5$  ps<sup>-1</sup> and an additional damping  $\eta_{\min}$  due to multiphonon processes and the creation of electron–hole pairs in the substrate. In our simulations, we used a reasonable estimate for an adsorbed atom,<sup>42</sup>  $\eta_{\min} = 0.01\omega_s$ , where  $\omega_s = [V_{SS}'(r_{SS})/m_S]^{1/2} \approx 41.9$  ps<sup>-1</sup> is a characteristic frequency of the substrate.

Finally, initial configurations were prepared from disordered high-temperature configurations by annealing with the temperature slowly decreasing toward  $T = 300$  K. This results in a liquid or amorphous film as a typical initial state.

### 3. RESULTS

**3.1. Structure of the Confined Water Film.** Before investigation of frictional properties, one has to determine the equilibrium structure of the confined water film. In this subsection we show how the structure of the water film, consisting of  $N_{\text{H}_2\text{O}} = 336$  molecules, changes with variation of the applied pressure  $f_1$  and the interaction between the water and substrates  $V_{SO}$ .

The equilibrium MD runs proceed as follows. We start from the lowest value of the load force  $f_1 = 10^{-3}$  eV/Å ( $f_1 = 10^{-2}$  eV/Å for smaller  $V_{SO}$  values) and anneal the system at  $T = 300$  K during the time period of 20 ps, and then, also during 20 ps, we measure the total potential energy of the system and the position of the top substrate  $z$  which characterizes the thickness of the lubricant film. We checked that this time is sufficient for our system to reach equilibrium (longer equilibration times of 80 ps were also used for  $V_{SO} > 0.05$  eV). Then we increase the applied load by the logarithmically equidistant steps up to the maximum value  $f_1 = 10$  eV/Å, repeating at every step the measurements described above. After that, the whole procedure is repeated during the decrease of the load back to  $f_1 = 10^{-3}$  eV/Å. Note that in the following we only show the data for the load

forces below  $f_1 = 1$  eV/Å (i.e., pressures below 25.6 GPa) for the technical reason explained further in Section 3.7.

The results are presented in Figure 2. It shows that on increase of the applied load the film is always thicker than

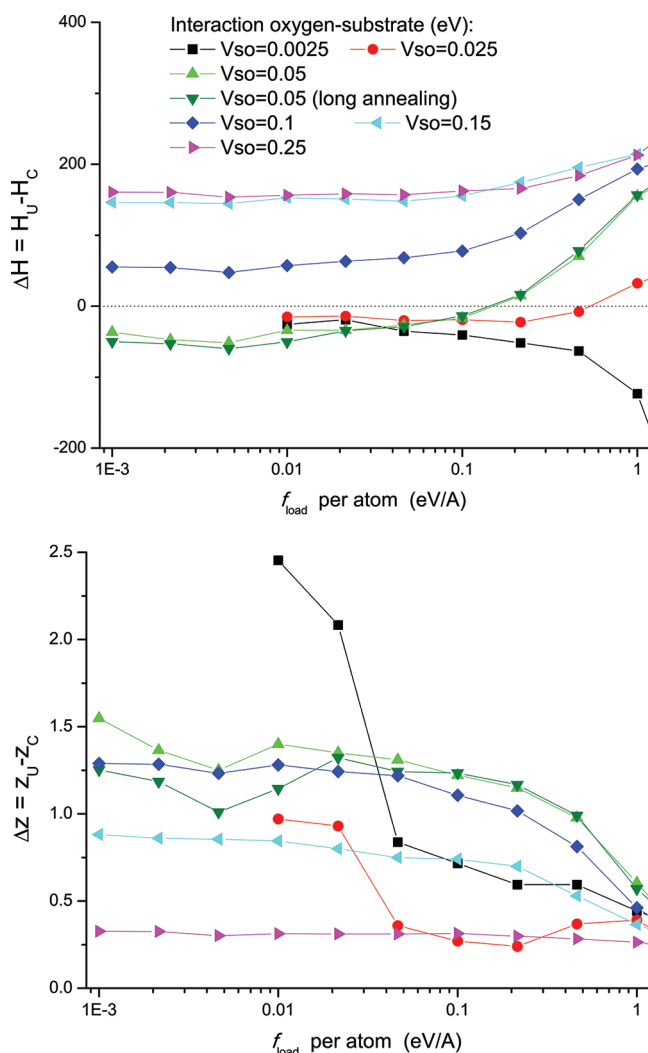


**Figure 2.** Total enthalpy  $\Delta H$  difference (top) and the difference in thickness  $\Delta z$  of the water layer (bottom) between the pairs of states at the same pressure, obtained on increase (U) and decrease (C) of the applied load  $f_1$  (via the procedure further described in the text) versus the applied load. The different symbols correspond to the different values of the interaction between the water molecules and the substrates  $V_{SO}$  as indicated in the legend.

during subsequent release of the load. That is why, in the following, we denote the former state as (U) (Uncompressed) and the latter one as (C) (Compressed). Both these (U) and (C) states represent roughly the most compressed and the most uncompressed metastable states in the system, at a fixed load (whereas the true ground state may lie somewhere in between). Since we are working at the condition of the controlled applied load, we can estimate their relative stability via the value of the total system enthalpy  $H = E + f_1 z$ , where  $E$  is the total potential energy of the system and  $z$  is its thickness. We found that, if the interaction of the water with the substrates is high enough,  $V_{SO} > 0.1$  eV, the (C) state during the release of the load is energetically preferred over the (U) one, obtained during progressive increase of the load, as

manifested by the positive  $\Delta H = H_U - H_C$  (Figure 2, top). This can be rationalized by the following argument. When the water film is more compressed, then more oxygen and hydrogen atoms interact simultaneously with both (top and bottom) substrates via the attractive part of the LJ potential. Therefore, if  $V_{SO}$  is high enough, this attraction results in the net decrease of the overall energy of the system, compared to the uncompressed state, even in spite of the increase of energy due to the repulsive core interaction between the H and O atoms because of compression of the water layer. By contrast, at the lowest  $V_{SO} = 0.0025$  eV, the (U) configuration is more stable at all loads. At the intermediate interval values of  $V_{SO} = 0.025$ – $0.05$  eV, the relative stability of the (U) and (C) configurations depends on  $f_1$  [(U) is more stable at lower loads, and (C) is more stable at higher loads].

Our plots of the film thickness and energy (Figure 2) are not able to resolve any sharp structural changes during compression/decompression. However, visual inspection of the atomic configurations suggests that the film can have several distinct structures. At lower loads  $f_1$  and water–substrate interactions  $V_{SO}$  the water film is always in the two-layer liquid state, which solidifies with the increase of the load (Figure 1, bottom). With the increase of the applied load and/or water–substrate interaction, the film is gradually transformed to a one-layer state (Figure 1, top), which can also contain a fraction of a “buckled” structure. The buckling of the very thin water film has earlier been observed in numerical experiments of the layer confined between two substrates with the change of the distance between the substrates at a fixed pressure.<sup>8,9</sup> The buckling emerges because the out-of-plane positions of the oxygen atoms in the buckled monolayer help to minimize the distortions of the hydrogen bonds. The complete phase diagram of the water confined between the flat surfaces has recently been calculated using the TIP4P model of water, and the place of the buckled “monolayer ice” phase in the diagram has been located.<sup>43</sup> Although we use a different model setup (the CF model for water, between atomically corrugated walls, and the fixed number of water molecules), we observe a similar buckled ice structure with the change of pressure and/or interaction with surfaces.

**3.2. Nondissociative Friction: Static and Kinetic Friction Forces.** In the friction experiments, we slowly increase the driving velocity  $v_s$  starting from zero to a given value, keeping the target Langevin temperature at  $T = 300$  K. Typical dependences of the spring force  $f$  (per one substrate atom) on time are presented in Figure 3. When the stage moves with a low velocity ( $v_s = 0.3$  Å/ps = 30 m/s), the spring elongates, and the force increases linearly with time until it reaches the value of the static friction force ( $f_s \approx 0.02$ – $0.04$  eV/Å). At this moment, the top substrate begins to slide and catches up with the stage, so that  $f$  decreases, the substrates stick again, and the whole cycle is repeated. This is the *stick–slip* regime shown in Figure 3a and Figure 3b. At a higher stage velocity ( $v_s = 3$  Å/ps = 300 m/s), the *smooth sliding* is observed (Figure 3c and Figure 3d), and the spring force is equal to the kinetic friction force  $f_k$ .

We present in this section the simulation results for the case of “hydrophilic” substrates ( $V_{SO} = 0.05$  eV), where the relative stability of the (U) and (C) configurations depends on the load  $f_1$  (Figure 2); namely, at  $f_1 < 0.1$  eV/Å, the uncompressed (U) state is more stable, while for  $f_1 > 0.1$  eV/Å the compressed (C) one is more stable.

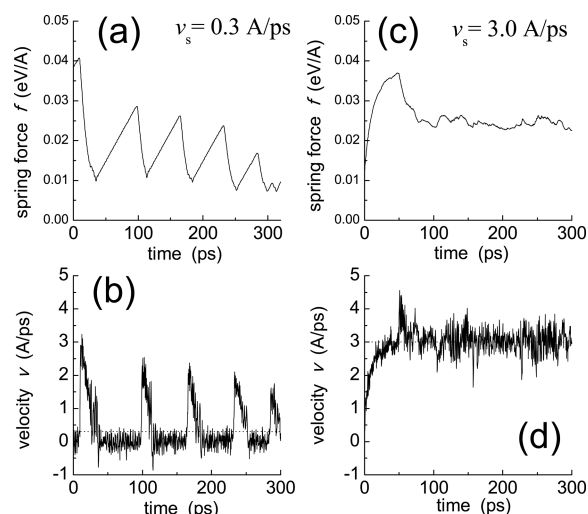


**Figure 3.** Typical time dependences of the spring force [panels (a) and (c)] and the velocity of the upper substrate [panels (b) and (d)] for the regimes of stick–slip motion [panels (a) and (b)] and smooth sliding [panels (c) and (d)]. The values of the driving velocity are  $v_s = 0.3$  Å/ps [(a) and (b)] and 3 Å/ps [(c) and (d)]. The parameters are  $V_{SO} = 0.05$  eV,  $N_{H_2O} = 336$ , and  $f_1 = 1$  eV/Å.

Starting from both (U) and (C) configurations with  $N_{H_2O} = 336$  obtained during the equilibrium loading/unloading runs described above (Section 3.1), we measured static  $f_s$  and kinetic  $f_k$  friction forces as functions of the applied load  $f_1$ . The results are presented in Figure 4.

Static and kinetic frictional forces stay approximately constant up to the load  $f_1 \approx 0.1$  eV/Å, for both the (U) and (C) initial configurations. For the more stable (U) configurations (solid symbols and curves in Figure 4), the structure of the film always corresponds to two layers, up to the load  $f_1 \approx 0.1$  eV/Å. The lubricant film is always solidified, as it is attested by nonzero values of the static friction force  $f_s \approx 0.02$ – $0.03$  eV/Å. During slips in the stick–slip regime (at lower driving velocities), the film does not melt, and it advances approximately half the distance traveled by the top substrate. Thus, the stick–slip is governed by inertia effects. At higher driving velocities, the system exhibits smooth sliding. At a lowest load,  $f_1 = 10^{-3}$  eV/Å, the smooth motion corresponds to the “layer–over–layer” sliding, accompanied by noticeable diffusion of water molecules between the lubricant layers. At higher  $f_1$  values, the lubricant remains solid during the sliding regime, and the film moves as a whole. In both cases, the sliding is *symmetric* (the film in average moves with half of the top substrate velocity,  $v_{\text{film}} \approx v_s/2$ ), and the kinetic friction force  $f_k \approx 0.02$  eV/Å is approximately equal to the static one.

The structure and frictional behavior of the compressed (C) configurations (open symbols and dotted curves in Figure 4) are different. At the low load  $f_1 < 0.1$  eV/Å, the lubricant film always has the “buckled one-layer” structure (Figure 1 top), which is metastable with respect to the two-layer (U) configuration. It also shows stick–slip motion at lower driving velocities and smooth sliding at higher driving velocities, with approximately two times higher values of both static and kinetic friction forces as compared with those for the (U) initial configurations. Now, however, the kinetic friction force ( $f_k \approx 0.033$  eV/Å) is smaller than the static one ( $f_s \approx 0.045$  eV/Å). An important difference from the (U) case is that now the sliding is *asymmetric* both during the slips in the stick–slip

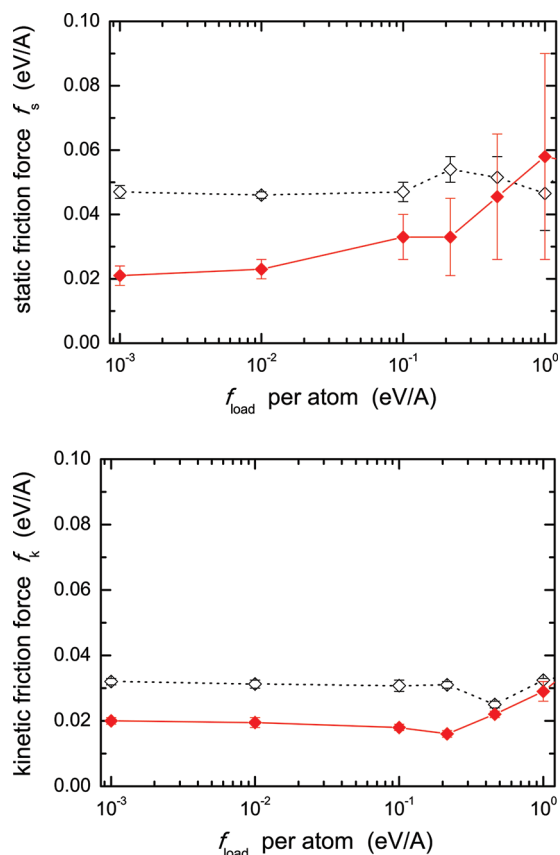


**Figure 4.** (Top) Static friction force  $f_s$  versus the applied load  $f_1$  for  $N_{\text{H}_2\text{O}} = 336$  and  $V_{\text{SO}} = 0.05$  eV. Solid symbols and curve indicate the friction force obtained from the uncompressed (U) configurations, while open symbols and dotted curve denote the friction force obtained from the compressed (C) ones. The highest/lowest values of the friction force found in the simulation runs are denoted with the “error bars”. (Bottom) The same for the kinetic friction  $f_k$  at the driving velocity  $v_s = 3$  Å/ps.

regime and in the smooth sliding regime. The water film moves, being attached to one of the substrates. The increase of both the static and kinetic friction forces for the (C) configurations as compared to the (U) ones can be explained in the following way. Let us consider the number of bonds participating in the interaction of the film with the substrates. While in the two-layer (U) film only half of water molecules interact with a substrate, this fraction is much larger than 0.5 (and approaches  $\sim 1$ ) for the film in the (buckled) one-layer configuration. Therefore, when the film moves, the rate of the breaking/forming of these bonds is much higher for the case of the (C) state, resulting in the increase of the friction forces.

Now let us describe the friction properties at higher loads  $f_1 > 0.1$  eV/Å, where the relative stability of the (U) and (C) states is reversed [(C) is now more stable]. As one can see from Figure 3, the static friction force decreases directly in the course of the stick–slip motion. This decrease is associated with the structural transition in the driven lubricant film; namely, initially the film had the same “buckled structure” as that of Figure 1 (top), which is characterized by a high static friction force  $f_s \approx 0.04$  eV/Å. However, already after the first few slips, the film restructures itself toward a flatter structure, which is characterized by a much lower value of the static friction force  $f_s \approx 0.02$  eV/Å (such a decrease of the friction force is denoted with the “error bars” in Figure 4). Note that the tendency of the

lubricant film to self-organize into a low-friction phase has also been observed in a simple system of Lennard-Jones atoms<sup>44</sup> as well as in a more realistic MD simulation of a dodecane film confined between mica surfaces.<sup>45</sup>

Therefore, at lower loads  $f_1 < 0.1$  eV/Å, the more stable (U) state always has smaller friction than the metastable (C) state, while the latter state shows no tendency for transition to (U) in the course of sliding. The situation at higher loads is not so clear. In particular, the question whether the flattening of the sliding layer observed immediately in the course of sliding corresponds to a structural change that is also the energetically favorable one in the equilibrium requires further investigation.

**3.3. Dependence of the Friction Force on the Number of Water Molecules.** Now let us vary the number of water molecules confined between the “hydrophilic” surfaces to see how it affects the friction of the water film. For this purpose, we extended the sliding experiments of Section 3.2 to different numbers of water molecules in the lubricant layer  $N_{\text{H}_2\text{O}} = 294, 315, 336, 357, 378, 399,$  and  $420$ . We start these runs from the uncompressed (U) configurations at the load value  $f_1 = 1.0$  eV/Å. The results for the friction forces are presented in Figure 5

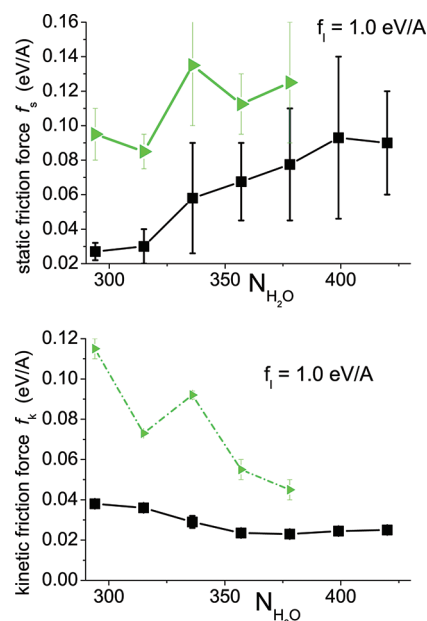


**Figure 5.** Static friction force  $f_s$  (top) and kinetic friction force  $f_k$  (bottom, measured at the driving velocity  $v_s = 3$  Å/ps) under the load of  $f_1 = 1.0$  eV/Å versus the number of water molecules in the lubricant layer  $N_{\text{H}_2\text{O}}$  for two values of the water–substrate interaction,  $V_{\text{SO}} = 0.05$  eV (black) and  $V_{\text{SO}} = 0.0025$  eV (green). The highest/lowest values of the friction force found in the simulation runs are denoted with the “error bars”.

(black lines and symbols). As one can see, the static and kinetic friction forces change in antiphase: while the static friction force  $f_s$  grows monotonically with  $N_{\text{H}_2\text{O}}$ , the kinetic friction force  $f_k$  demonstrates an overall decrease with  $N_{\text{H}_2\text{O}}$ , exhibiting also a weak minimum near  $N_{\text{H}_2\text{O}} \approx 380$ .

These dependences can be understood in terms of the variation of the structure of the water lubricant film. At the lowest value of  $N_{\text{H}_2\text{O}} = 294$ , the structure of the water film is one layer, similar to that depicted in Figure 1 (top), but without any buckling, while at the largest number of the water

molecules  $N_{\text{H}_2\text{O}} = 420$ , the water layer has two well-defined layers, as in Figure 1 (bottom). Beginning from  $N_{\text{H}_2\text{O}} = 315$  up to  $N_{\text{H}_2\text{O}} = 378$ , the water film structure gradually changes from one to two layers. Thus, the decrease of the kinetic friction force  $f_k$  with  $N_{\text{H}_2\text{O}}$  can be explained by the number of water molecules in the immediate contact with the substrates (and therefore by the number of “hydrogen bonds” per unit area per unit time that are broken/created during sliding). While there are all  $N_1 = 294$  water molecules in contact with both substrates in the flat layer with  $N_{\text{H}_2\text{O}} = 294$ , this number strongly decreases to  $N_2 = 189$  for the *two-layer* film with  $N_{\text{H}_2\text{O}} \approx 378$ , and then it weakly increases proportional to  $N_{\text{H}_2\text{O}}$ . The ratio of  $N_1/N_2 \approx 1.6$  corresponds very well to the ratio of the highest/lowest values of the kinetic friction force  $f_k$  encountered in Figure 5.

On the other hand, the static friction force  $f_s$  depends mainly on the energy barriers that the system needs to overcome to initialize the motion, i.e., on the “roughness” of the lubricant film. The observation that the static friction force increases monotonically during the transition from one to two layers in the water film in our experiments suggests that the roughness of the film increases, on average, as one goes from one lubricant layer to two layers, with a rougher, less dense arrangement of the water molecules within the layers. Besides, as it has already been pointed out in the previous section, the film generally restructures itself toward a more flat configuration immediately in the course of sliding, which explains large error bars seen in Figure 5 (top).

**3.4. Dependence of the Friction on the Interaction of Water with Substrates.** Next, let us consider the case of the “hydrophobic” surfaces and repeat the simulations described in the previous Section 3.3 at  $V_{\text{SO}} = 0.0025$  eV and  $N_{\text{H}_2\text{O}} = 294, 315, 336, 357,$  and  $378$ , starting in all cases from the (U) configurations of the lubricant film. At  $V_{\text{SO}} = 0.0025$  eV, the (U) configurations are always more stable with respect to the (C) ones (Figure 2).

While the overall behavior during these runs is the same as described in Section 3.2 (stick–slip motion with a transition to smaller values of the static friction force at lower driving velocities and smooth sliding at higher driving velocities), the values of both static and kinetic friction forces are systematically higher (2 to 4 times) for all water film thicknesses, as shown in Figure 5 (green lines and symbols). One can also note in Figure 5 that the increase of friction for the case of “hydrophobic” substrates is not uniform; i.e., a particular water surface concentration that corresponds to  $N_{\text{H}_2\text{O}} = 336$  and  $N_{\text{H}_2\text{O}} = 294$  brings a stronger increase in both static and kinetic friction forces.

Initial insight into such behavior can be obtained merely from the inspection of atomic configurations. Typical snapshots during sliding under the load  $f_1 = 1$  eV/Å are shown in Figure 6b for “hydrophilic” surfaces and Figure 6a for “hydrophobic” surfaces.

In the “hydrophilic” case, Figure 6b, the water molecules form, during sliding, almost a purely *flat* structure, with only some minor buckling. In the “hydrophobic” case, Figure 6a, more water molecules are protruding toward the substrates from both upper and lower surfaces of the lubricant layer, thus forming much rougher, “zig-zag-like” arrangements. Namely, this *rougher morphology* of the water layer in contact with the

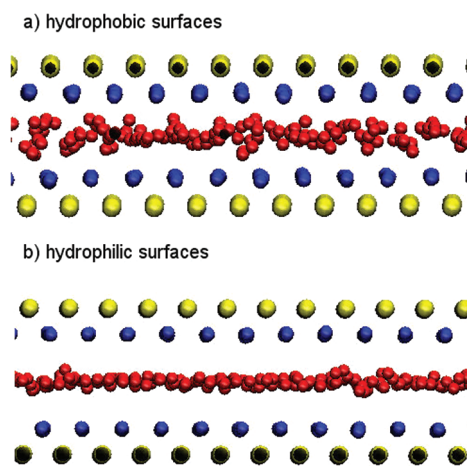


**Figure 6.** Side views (across the driving direction) of typical atomic configurations for the cases of “hydrophobic” (a) and “hydrophilic” (b) surfaces. Only oxygen atoms are shown in the water molecules. The parameters are  $N_{\text{H}_2\text{O}} = 336$  and  $f_1 = 1$  eV/Å.

“hydrophobic” surfaces is one of the reasons for the increase of both static and kinetic friction in this case.

To understand, in more detail, how the potential landscape of the substrates for the water molecules affects the structure/friction of the water layer, we plot the total potential energy of an oxygen atom near one substrate surface versus its  $z$ -coordinate. Such a surface, resembling the ones we use in MD runs, consists of two rigid substrate layers of the same square structure as in the simulation that are separated from each other by 1.6 Å, as obtained from the simulations at the load  $f_1 = 1$  eV/Å. At a fixed  $z$ -position of an oxygen atom, the potential landscape (e.g., originating from the bottom surface) is obviously periodic in  $x$  and  $y$  directions with the periodicity of the substrate. The values of the minimum and maximum energy of such a landscape of the bottom substrate,  $E_{\text{min}}(z)$  and  $E_{\text{max}}(z)$ , as functions of  $z$  are plotted in the Figure 7 with the dotted lines for both “hydrophilic” and “hydrophobic” cases. At a fixed energy level,  $E = \text{const}$ , the difference in  $z$  positions,  $\Delta z$ , of the points belonging to the lines of the minimum and maximum energies,  $E_{\text{min}}(z)$  and  $E_{\text{max}}(z)$ , respectively, represents a sort of spatial corrugation of the substrate surface, as seen by an oxygen atom having this certain energy  $E$ . By comparing the  $\Delta z$  data for both “hydrophobic” and “hydrophilic” surfaces (Figure 7, dotted lines, top vs bottom plots), we observe that for the “hydrophobic” substrate  $\Delta z$  is systematically higher.

Furthermore, in Figure 7 we plot also (with the points) the actual data from the simulation snapshot ( $N_{\text{H}_2\text{O}} = 336$ ,  $T = 300$  K, and  $f_1 = 1$  eV/Å) that correspond to all the oxygen and hydrogen atom interaction energies with the top (black symbols) and the bottom (red symbols) substrates in the absence of driving. As expected, these data points for oxygens near both “hydrophobic” and “hydrophilic” surface landscapes lie close to the minimum energy dotted curves. The highest energies attained by oxygens due to their interaction with the bottom substrate are  $\approx 1$  eV in the “hydrophobic” case and  $\approx 0.5$  eV in the “hydrophilic” case. At these energy levels, the difference in the corrugations of the potential landscapes amounts to  $\Delta z_{\text{phobic}} - \Delta z_{\text{philic}} \approx 0.2$  Å, which provides the room for a “rougher” water layer structure in the “hydrophobic” case visible in Figure 6. It should be noted here that we do not expect a similar effect of increased lubricant layer “roughness”

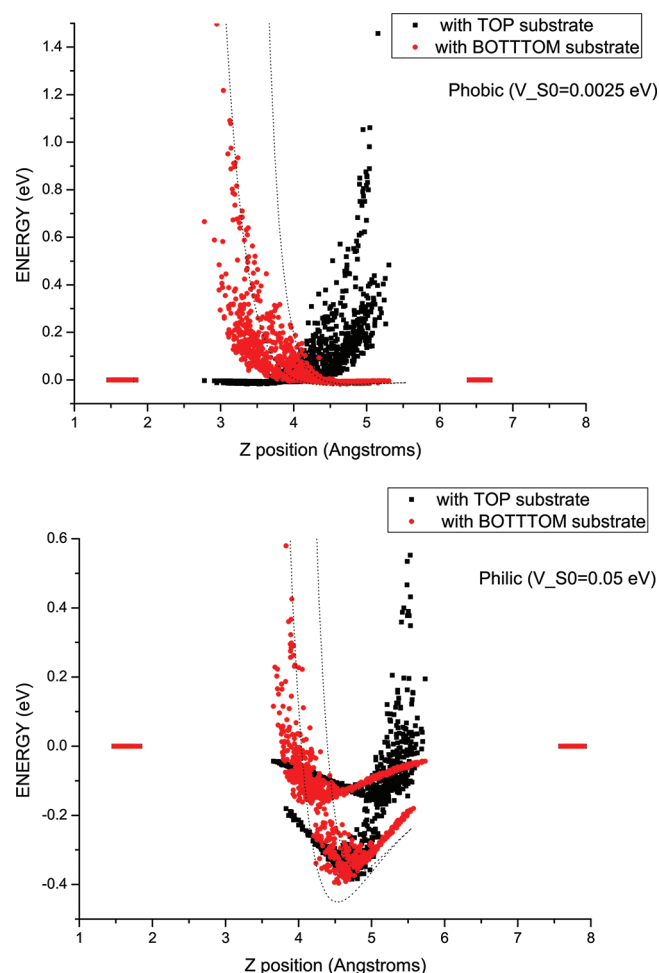


**Figure 7.** Total energies of the interaction of the oxygen and hydrogen atoms with the “hydrophobic” (upper plot) and “hydrophilic” (lower plot) surfaces. The dotted lines show minimum and maximum energies,  $E_{\min}(z)$  and  $E_{\max}(z)$ , of the interaction of an oxygen atom with the two-layer bottom substrate (obtained by varying the lateral  $(x,y)$  position of the atom), as functions of  $z$  (the substrate is assumed to be infinitely rigid). The symbols show the actual interaction energies obtained from a simulation snapshot with  $N_{\text{H}_2\text{O}} = 336$ ,  $T = 300$  K, and  $f_1 = 1$  eV/Å in the absence of driving. The black symbols indicate the interaction energies with the top substrate and the red symbols with the bottom substrate. Two visible branches of each color, where the points group together, correspond to the oxygen and hydrogen atoms. The isolated groups of points at zero energy in both extremities of the abscissa axes correspond to the atoms of the top and bottom flexible substrates.

to happen in the case where the lubricant consists of simple Lennard-Jones particles because in our opinion it is the unique competition of the corrugation imposed by the substrates and the internal structure of the water (which tends to form zigzag-like structures) that brings this “roughness” effect.

**3.5. Dissociative Friction.** In principle, the increased corrugation of the “hydrophobic” substrates alone could rationalize the occurrence of the enhanced (2 to 4 times) friction. However, there is another process that comes into play and leads to the overall increase in friction—the *dissociation of the water molecules that occurs readily in the course of frictional sliding events.*

To quantify the dissociation processes, we use the following measurements. First, we set up the “static” OH bonds (i.e.,

those intramolecular bonds that exist in the very beginning of the friction runs in the absence of driving). Initially there are  $2N_{\text{H}_2\text{O}}$  of such “static” bonds that correspond to  $N_{\text{H}_2\text{O}}$  well-defined water molecules. Then we follow the evolution of the number of “static” bonds during frictional sliding. We consider such a “static” bond to be irreversibly broken if its length exceeds  $3R_{\text{OH}}$ , where  $R_{\text{OH}} \approx 0.96$  Å is the equilibrium OH bond distance in the water molecule. Thus, we are able to obtain the information about the *forward rate* of dissociation. Second, we determine the number of the instantaneous, “dynamic” OH bonds. This quantity shows the *apparent level* of water ionization, which results from both the dissociation and recombination reactions. After some testing, the cutoff distance for the “dynamic” OH bonds was taken as  $\leq 1.4R_{\text{OH}}$ , which allows us to filter out intermolecular hydrogen bonding that is characterized by the length  $\approx 1.8R_{\text{OH}}$ . At the same time, such a cutoff distance can reliably identify the  $\text{H}_3\text{O}^+$  groups characterized by slightly longer OH bonds, compared to those in the OH and  $\text{H}_2\text{O}$  groups. During the time evolution, we keep track of oxygen atoms having 1, 2, and 3 such “dynamic” OH bonds, which shows the instantaneous quantities of the OH,  $\text{H}_2\text{O}$ , and  $\text{H}_3\text{O}^+$  groups in the system (while we observe almost no other, spurious, groups such as H or  $\text{H}_4\text{O}$ ).

Time evolution of the “static” and “dynamic” OH bonds in the system during frictional sliding is demonstrated in Figure 8. Namely, panel (c) shows the number of “static” OH bonds and their time derivative (which is proportional to the forward rate of dissociation), while panel (d) shows the instantaneous numbers of OH,  $\text{H}_2\text{O}$ , and  $\text{H}_3\text{O}^+$  entities in the system. In the same figure, the spring force and the velocity of the top rigid substrate are plotted (panels (a) and (b)). We show the portion of the friction run at  $v_s = 1.0$  Å/ps, followed by the one at  $v_s = 3.0$  Å/ps, and the driving velocity  $v_s$  is increased sharply at  $t = 328$  ps. One can notice (Figure 8c) that the dissociation occurs in bursts during the slip events of the stick–slip regime, at lower driving velocity, while it also continues in the smooth sliding regime, at higher driving velocity. Furthermore, the average rate of dissociation of the “static” OH bonds is roughly proportional to the driving speed (0.37 bonds/ps for  $v_s = 1.0$  Å/ps versus 0.84 bonds/ps for  $v_s = 3.0$  Å/ps). The dissociation proceeds via the detachment of one hydrogen, which may diffuse many Angstroms away from its “parent” oxygen, so that by the end of the run shown about 400 out of 672 initial static bonds are irreversibly broken.

By contrast, the apparent level of dissociation observed is not high due to the recombination processes as shown in Figure 8d. Only  $\approx 25$  hydroxide OH and  $\approx 25$  hydronium  $\text{H}_3\text{O}^+$  groups continuously persist in the system of 336 water molecules throughout the run, while the remaining oxygens form  $\approx 286$  well-defined  $\text{H}_2\text{O}$  molecules. Of course the exact quantities are somewhat cutoff-dependent, but the chosen cutoff yields the best approximation for the standard water ionization reaction  $2\text{H}_2\text{O} \leftrightarrow \text{OH}^- + \text{H}_3\text{O}^+$ . Moreover, we can estimate the molar concentration of both  $\text{OH}^-$  and  $\text{H}_3\text{O}^+$  groups in our system as  $\approx 7$  mol/L, which is about 8 orders of magnitude higher than the self-ionization values for water ( $10^{-7}$  mol/L). This attests the strength of the frictional shear effect on the water molecules. The temperature of the water film in these runs increased up to 340 K only.

These findings raise the question to what extent the observed dissociation of water is responsible for the increase

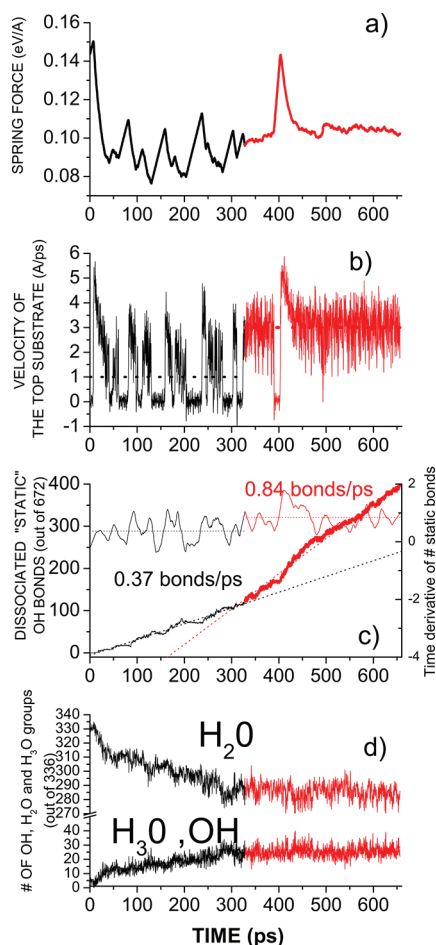


**Figure 8.** Plots of the friction force (a), the velocity of the top substrate (b), the total number of static dissociated OH bonds and the time derivative of it (details in the text), (c) and the total number of dynamic OH, H<sub>2</sub>O, and H<sub>3</sub>O atomic groups (d) in the system versus time. At the time  $t_{sw} \approx 328$  ps the velocity of driving  $v_s$  has been increased from 1.0 to 3.0 Å/ps (the curves are plotted in black and red to distinguish this time point). Other parameters are:  $N_{H_2O} = 336$ ,  $T = 300$  K, and  $f_1 = 1$  eV/Å.

of the friction forces. It is quite reasonable to suppose that the breaking of the strong OH bonds during sliding should lead to the increase of both kinetic as well as static friction forces (since the dissociation was observed also during the slip events in the stick–slip regime). It is not easy to separate, however, the two effects (those of dissociation and increased substrates corrugation) clearly. In an attempt to do so, we completed also the runs at a slightly lower load  $f_1 = 0.46$  eV/Å (all other parameters are kept the same). In these latter runs, the dissociation of water was much weaker, and we assumed that the effect of enhanced corrugation of the “hydrophobic” substrate is responsible alone for the  $\approx 1.5$  times increase in friction. Roughly presuming that the enhanced corrugation has the same effect at a higher load  $f_1 = 1.0$  eV/Å, where a total 2- to 4-fold increase of friction is observed, we can estimate that the dissociation processes enhance friction on average two times in our runs at  $f_1 = 1.0$  eV/Å.

Further support for the link between the dissociation and enhanced friction is obtained from Figure 9, where the static and kinetic friction forces for the “hydrophobic” surfaces and for a different number of water molecules  $N_{H_2O}$  from Figure 5

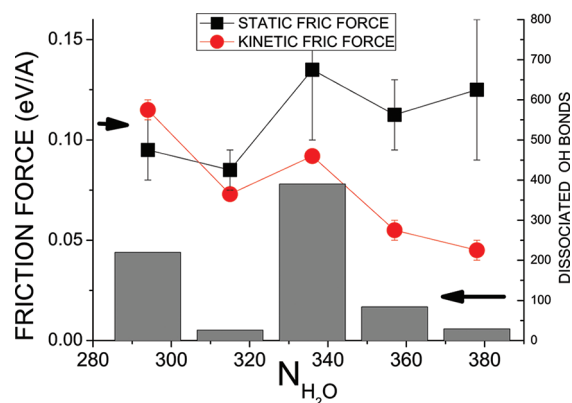


**Figure 9.** Static and kinetic friction forces from Figure 5 plotted alongside the number of the dissociated OH bonds at the end of the 328 ps run with  $v_s = 3.0$  Å/ps (details in the text). Other parameters are:  $T = 300$  K and  $f_1 = 1$  eV/Å.

are replotted. Besides, Figure 9 shows the total number of dissociated static OH bonds by the end of the runs similar to the one depicted in Figure 8. One can notice that both the increase of friction and the dissociation are not uniform, and for some values of  $N_{H_2O}$ , such as  $N_{H_2O} = 294$  and  $N_{H_2O} = 336$ , they are stronger than for the others. While we did not analyze in detail this effect in terms of commensurability/incommensurability between the structures of the water layer and the substrates (it turns out to be difficult because the water layer is largely disordered), here we emphasize the correlation between the friction and the dissociation.

**3.6. Dependence on the Frictional Properties on the Orientation of the Substrates.** In realistic situations, the confining substrates never match perfectly; i.e., they usually have different structures or lattice constants or may be rotated with respect to each other. In their study, Müser et al.<sup>35,36</sup> have shown that perfectly matching substrates may lead to the reduction kinetic and enhanced static friction forces, compared to the generic case of the nonmatching substrates. To eliminate the concerns that perfectly matching substrates may affect our results, we repeated many of our simulations described above for the setup where the atomic lattice of the bottom substrate has been rotated by some angle ( $\approx 31^\circ$ ) and also deformed slightly to fit perfectly into the simulation box (for details see ref 37). While the majority of results obtained in these series of simulations is beyond the scope of the current paper, we mention only that such modification of the setup did not alter qualitatively any of our results reported here. Overall, we found both static and kinetic friction forces to be slightly lower for the rotated substrates case. Thus, the results reported in the present paper are robust against such a modification of the system, and they should be valid also for the more realistic case of nonmatching substrates.

**3.7. Deformation of Substrates during Frictional Sliding at High Load Forces.** As mentioned in the Introduction, the higher pressure values we used in our simulations (tens of gigapascals) lie already within the range of yield strengths of common inorganic materials such as steel, quartz, diamond, etc. Moreover (Section 2), for the interaction between the substrate atoms, we chose the parameters to mimic approximately the strength of a quartz-like material (though both the structure and the energetic model for the substrates are extremely simplified). Therefore, a plastic behavior of the substrates might be expected to occur in the course of our

simulations. We have not observed it at the equilibrium compression/decompression runs, up to the load forces  $f_1 \sim 10$  eV/Å, described in Section 3.1, nor has it been seen during the nonequilibrium frictional runs at the lower range of pressures  $f_1 < 1$  eV/Å. However, at  $f_1 \geq 1$  eV/Å and for the “hydrophobic” substrates only, we have observed in a couple of runs that the substrates can occasionally be deformed irreversibly during the frictional sliding, with the “bridges” of the “flexible substrate” atoms forming between two moving surfaces, thus drastically increasing the friction and effectively welding the surfaces together (see Figure 10). While this behavior may be

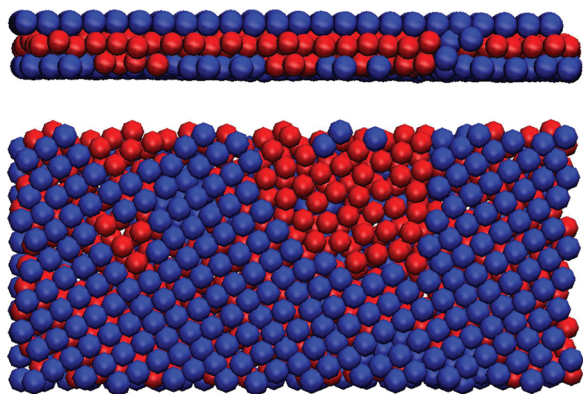


**Figure 10.** Side and bottom view of the atomic configuration obtained during frictional sliding at high compressive force  $f_1 = 1$  eV/Å at the end of the 328 ps run with  $v_s = 0.3$  Å/ps. Only the oxygen atoms of water molecules (red spheres) and flexible atoms of the substrates (blue spheres) are shown. The plastic deformation of the lower substrate is apparent.

interesting on its own, for the purpose of the current paper, we took care that all the data reported above are taken from the runs where such frictional welding is not observed. For the same reason, we restrict the interval of the applied load by  $f_1 \leq 1$  eV/Å on all the graphs.

#### 4. DISCUSSION

In the present paper, we deal with thin water layers subjected to very high pressures (up to 25.6 GPa for  $f_1 = 1$  eV/Å) and strongly driven by moving surfaces. One may wonder whether novel, exotic states of matter can occur under such extreme conditions. In particular, in view of water dissociation processes that we observe, it is interesting to relate our findings to the peculiar “superionic” and “ionic fluid” states of water suspected to exist on giant planets Neptune and Uranus and modeled via ab initio MD methods by Cavazzoni et al.<sup>23</sup> and Goldman et al.<sup>24</sup> In the “superionic” phase of water, the mobility of oxygens decreases abruptly down to zero with the increasing pressure; thus, the oxygen atoms form a solid state, either crystalline or disordered, whereas the hydrogens remain highly mobile at all pressures. In a sense, the superionic phase can be termed as “partially melted”. Such a novel phase has been found to exist at pressures above 30 GPa and temperatures above 1000 K. Besides, the fully dissociated “ionic fluid” state has been found to exist at yet higher pressures and temperatures.

Our simulations are carried out at the room ambient temperature, and in the friction runs the temperature has never been found to increase past 600 K (e.g., it increased only up to 340 K in the run reported in Figure 8). Nevertheless, the strong frictional driving together with the extreme confinement have a

dissociating effect on water molecules, similar to the effect of high temperatures.

Furthermore, in the friction studies, when the lubricant is confined within a thin film, it is often difficult to distinguish between the solid and the liquid states of such a film. The best estimate is the comparison of the mobilities or diffusivities of the species. Besides, the film itself moves past both surfaces in the driving direction  $x$  (usually with the average drift velocity  $v_{\text{drift}} = 0.5v_s$ ). Some preliminary assessment about mobilities of the oxygens and hydrogens can be made from the analysis of their trajectories in the  $(x,y)$  plane, such as those depicted in Figure 11 (top). It shows that the mobility of the hydrogen

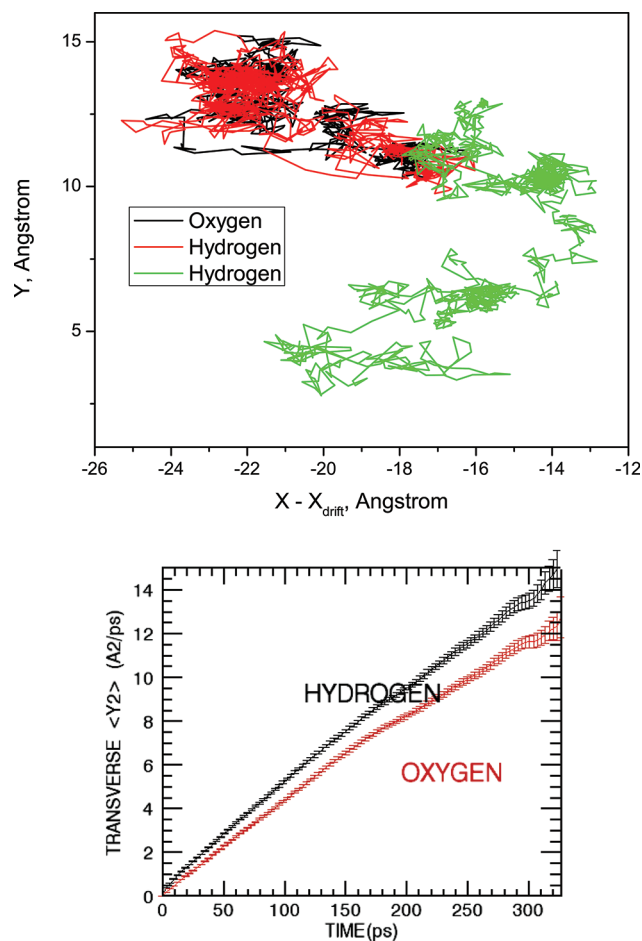


**Figure 11.** Top:  $(x,y)$  plane atomic trajectories of one oxygen and two hydrogen atoms, initially belonging to one molecule, picturing the dissociation event ( $x$  is taken relative to a steady drift value  $x_{\text{shift}}(t) = v_{\text{drift}}t$  for the whole water film). The data are taken from the run shown in Figure 8. Bottom: the average square of the transverse displacement  $\langle y^2 \rangle$  for oxygen and hydrogen atoms during the same run.

atom dissociated from its “parent” oxygen is higher than the mobility of the oxygen and the remaining hydrogen.

The square of the transverse displacement  $\langle y^2 \rangle$  averaged over all the oxygen and all the hydrogen atoms present in the run from Figure 8 is plotted in Figure 11 (bottom). It does show the enhancement of the diffusivity for hydrogen atoms on average (even though the large fraction of them are still found in the state bound to oxygens in the data used). The estimation from Figure 11 (bottom) gives for the transverse diffusivities  $D_{\text{H},y} \approx 2.4 \times 10^{-6}$  cm<sup>2</sup>/s and  $D_{\text{O},y} \approx 2.0 \times 10^{-6}$  cm<sup>2</sup>/s, while the analogous estimation for the longitudinal (in the direction of

driving) diffusivities gives  $D_{H,x} \approx D_{O,x} \approx 10^{-5}$  cm<sup>2</sup>/s. In comparison, in the absence of water dissociation in our frictional runs, we have  $D_H = D_O < 10^{-7}$  cm<sup>2</sup>/s, both in the longitudinal and in the transverse directions, while for the “superionic” states of water one finds  $D_H \sim 10^{-5}$  cm<sup>2</sup>/s and  $D_O \ll 10^{-5}$  cm<sup>2</sup>/s.<sup>23,24</sup> As one can see, the dissociation of water molecules does lead to the increase of diffusivities by some 2 orders of magnitude. Furthermore, the diffusivities for both hydrogens and oxygens in our frictional runs are close to those found for the “superionic” water hydrogens, even though the dissociation in our runs is far from complete. It is natural to expect a faster diffusion of the dissociated hydrogen atoms merely due to their smaller mass. However, the notable difference from the “superionic” water is that in our case the oxygen subsystem is not “frozen”, even though it does show smaller diffusivity than the hydrogen subsystem. This is the result of the external driving. One cannot exclude that in some other regimes of driving, not explored in the present paper, the oxygen subsystem can remain “frozen”, in a complete similarity to the “superionic” water, while the combined effect of driving and pressure still gives rise to the “superionic” dissociated hydrogen.

Thus, one can hypothesize that in our friction study we observe the precursor to (or the manifestation of) the same dissociative behavior that has been seen in the bulk equilibrium simulations of water at high pressures via ab initio MD methods, while this behavior is modified by the presence of the external driving. Indeed, we do observe that the rate of dissociation is roughly proportional to the speed of driving, and one needs quite high driving velocities (of the order of meters/second) to achieve noticeable dissociation. In many generic friction systems, the macroscopic driving speeds are many orders of magnitude slower (micrometers per second). However, the bursts of fast movements of the substrates, leading to dissociation of the water confined between them, may readily occur even in such systems, during the slip events in the “stick–slip” regime of friction. Besides, in many other situations that become increasingly important in practice, the fast speeds of driving of the order of many meters per seconds can be easily achieved (e.g., in a hard-disk drive of the radius  $R \sim 3$  cm with the rotation speed of  $\omega \sim 7200$  rpm, the linear speed at the edge of a platter is  $2\pi R\omega \sim 20$  m/s).

It is also interesting to put one- and two-layer liquid and solid (amorphous) water structures we observe (Figure 1) in some correspondence with the equilibrium phases of water. While we did not observe any particular crystalline order in our simulations, we can roughly estimate the density of the water film. For example, the data in Figure 7 show the  $z$ -positions of the centers of all H and O atoms belonging to the water film, at the load force  $f_1 = 1.0$  eV/Å (pressure of 25.6 GPa). This film has a solidified buckled one-layer structure, similar to that shown in Figure 1 (top), and the coordinates of all H and O atom centers span the interval of 2.0–2.6 Å thick (depending on the strength of the water–substrate interaction). One can take the midpoints of the “gaps” between the water layer and the top and bottom flexible substrates as the measure of the water layer thickness (the atoms belonging to both flexible substrates are visible as the isolated groups of points at zero energy in both extremities of the abscissa axes in Figure 7). This gives the total thickness of the water layer as 3.5–3.8 Å, which corresponds to a density of 1.7–1.9 g/cm<sup>3</sup>. This estimate lies in the plausible range for the ice VII at high pressures of tens of GPa (e.g., ice VII has the density of 1.65 g/cm<sup>3</sup> at 2.5

GPa and 300 K<sup>46</sup>). At lower pressures, we are able to see a range of gradually decreasing water density down to the standard 1.0 g/cm<sup>3</sup>; however, with our present data, we could not distinguish any plateau on the density versus pressure dependence (that would correspond to the well-defined crystalline ice phases, such as the ice VI).

Finally, let us note that, in our simulations, a water molecule dissociates, by construction of the CF model, into H<sup>+0.33</sup> and OH<sup>-0.33</sup> partial ions<sup>47</sup> instead of single electron charges. This tendency, however, does correspond to the average charge distributions obtained in recent ab initio calculations of high-pressure water.<sup>28</sup> Besides, the CF model is known to overestimate pressures by about 100 times<sup>40</sup> (around the normal pressure). Nevertheless, surprisingly, in our simulations, we arrive at the figure for the pressure at which the substantial dissociation is made possible (25.6 GPa) that almost matches the one (30 GPa) obtained in the ab initio modeling.<sup>23,24</sup> This suggests that actual pressures needed for dissociation in the nonequilibrium frictional runs (as opposed to the equilibrium situation) might actually be about 2 orders of magnitude lower, which may include the typical pressures in frictional sliding of a wide range of materials of intermediate hardness.

## 5. CONCLUSIONS

In the present paper, we reported the detailed MD study of the friction properties of the ultrathin water film confined between two solid surfaces in moving contact. With the increase of the load, the film is solidified (at room temperature) passing through two ice-like structures and taking finally a completely flat configuration.

The system demonstrates the transition from stick–slip to smooth sliding at an atomic-scale velocity of the order  $v_c \sim 1$  Å/ps = 100 m/s. The film remains solidified during slips; therefore, the stick–slip motion is governed by inertia effects contrary to the melting/freezing mechanism of oil-like lubricants. The film may be melted due to driving, but this occurs at a quite high driving velocity  $v_s > 1$ –10 Å/ps. Note that such features are similar to those observed for simple Lennard-Jones lubricants.<sup>33,34,48–51</sup>

We found that the “hydrophilic” surfaces demonstrate smaller friction with the water film than the “hydrophobic” surfaces. We explain this effect in terms of the increased corrugation of the “hydrophobic” substrates, which leads, at high pressures, to a rougher morphology of the water film too.

Depending on the applied load and on the strength of the interaction of water with the substrates, we have found two distinct friction scenarios—nondissociative and dissociative friction. In the latter scenario, the water molecules dissociate and recombine immediately in the course of sliding. The rate of such dissociation is found to be roughly proportional to the speed of driving. We estimate that the dissociation events lead to a roughly 2-fold increase of both static and kinetic friction force at  $f_1 = 1$  eV/Å due to the breaking of the OH bonds.

The relation of the observed frictional dissociation phenomena to the peculiar “superionic” and “ionic fluid” states of water<sup>23,24</sup> is discussed. We hypothesize that the states of water found in the thin lubricant film under high pressure and driven by moving substrates may be of the same nature as the above-mentioned states. Such partially melted “superionic” states are difficult to distinguish in the friction experiments; however, one can characterize them by the different diffusivities of the oxygen and hydrogen subsystems.

## ■ AUTHOR INFORMATION

## Corresponding Author

\*E-mail: obraun.gm@gmail.com.

## Notes

The authors declare no competing financial interest.

## ■ ACKNOWLEDGMENTS

S.C. thanks NSERC for funding this research. This work was made possible by the facilities of the Shared Hierarchical Academic Research Computing Network (SHARCNET: www.sharcnet.ca) and Compute/Calcul Canada.

## ■ REFERENCES

- (1) Persson, B. N. J. *Sliding Friction*; Springer-Verlag: New York, 1998.
- (2) Urbakh, M.; Klafter, J.; Gourdon, D.; Israelachvili, J. *Nature* **2004**, *430*, 525–528.
- (3) Petrenko, V.; Whitworth, R. *Physics of Ice*; Oxford University Press: USA, 2002.
- (4) Stanley, H. E.; Buldyrev, S. V.; Mishima, O.; Sadr-Lahijany, M. R.; Scala, A.; Starr, F. W. *J. Phys.: Condens. Matter* **2000**, *12*, A403.
- (5) Porter, J. D.; Zinn-Warner, A. S. *Phys. Rev. Lett.* **1994**, *73*, 2879.
- (6) Bergman, R.; Swenson, J. *Nature* **2000**, *403*, 283–286.
- (7) Meyer, M.; Stanley, H. E. *J. Phys. Chem. B* **1999**, *103*, 9728–9730.
- (8) Zangi, R.; Mark, A. E. *Phys. Rev. Lett.* **2003**, *91*, 025502.
- (9) Zangi, R.; Mark, A. E. *J. Chem. Phys.* **2003**, *119*, 1694–1700.
- (10) Koga, K.; Zeng, X. C.; Tanaka, H. *Phys. Rev. Lett.* **1997**, *79*, 5262.
- (11) Koga, K.; Tanaka, H.; Zeng, X. C. *Nature* **2000**, *408*, 564–567.
- (12) Slovak, J.; Tanaka, H.; Koga, K.; Zeng, X. C. *Phys. A* **2003**, *319*, 163–174.
- (13) Jagla, E. A. *Phys. Rev. Lett.* **2002**, *88*, 245504.
- (14) Raviv, U.; Laurat, P.; Klein, J. *Nature* **2001**, *413*, 51–54.
- (15) Raviv, U.; Klein, J. *Science* **2002**, *297*, 1540–1543.
- (16) Perkin, S.; Goldberg, R.; Chai, L.; Kampf, N.; Klein, J. *Faraday Discuss.* **2009**, *141*, 399–413.
- (17) Leng, Y.; Cummings, P. T. *Phys. Rev. Lett.* **2005**, *94*, 026101.
- (18) Stevens, M. J.; Grest, G. S. *Biointerphases* **2008**, *3*, FC13–FC22.
- (19) Paliy, M.; Braun, O.; Consta, S. *Tribol. Lett.* **2006**, *23*, 7–14.
- (20) Kalra, A.; Garde, S.; Hummer, G. *Eur. Phys. J.* **2010**, *189*, 147–154.
- (21) Huang, D. M.; Sendner, C.; Horinek, D.; Netz, R. R.; Bocquet, L. *Phys. Rev. Lett.* **2008**, *101*, 226101.
- (22) Sendner, C.; Horinek, D.; Bocquet, L.; Netz, R. R. *Langmuir* **2009**, *25*, 10768–10781.
- (23) Cavazzoni, C.; Chiarotti, G. L.; Scandolo, S.; Tosatti, E.; Bernasconi, M.; Parrinello, M. *Science* **1999**, *283*, 44–46.
- (24) Goncharov, A. F.; Goldman, N.; Fried, L. E.; Crowhurst, J. C.; Kuo, I.-F. W.; Mundy, C. J.; Zaug, J. M. *Phys. Rev. Lett.* **2005**, *94*, 125508.
- (25) French, M.; Mattsson, T. R.; Nettelmann, N.; Redmer, R. *Phys. Rev. B* **2009**, *79*, 054107.
- (26) Goldman, N. *J. Chem. Phys.* **2009**, *130*, 124517.
- (27) Kang, D. J. *Chem. Phys.* **2011**, *135*, 024505.
- (28) Wu, C. J.; Fried, L. E.; Yang, L. H.; Goldman, N.; Bastea, S. *Nat. Chem.* **2009**, *1*, 57–62.
- (29) Schwegler, E.; Sharma, M.; Gygi, F.; Galli, G. *Proc. Natl. Acad. Sci. U.S.A.* **2008**, *105*, 14779–14783.
- (30) Goncharov, A. F.; Sanloup, C.; Goldman, N.; Crowhurst, J. C.; Bastea, S.; Howard, W. M.; Fried, L. E.; Guignot, N.; Mezouar, M.; Meng, Y. *J. Chem. Phys.* **2009**, *130*, 124514.
- (31) Ikeda, T.; Katayama, Y.; Saitoh, H.; Aoki, K. *J. Chem. Phys.* **2010**, *132*, 121102.
- (32) Katayama, Y.; Hattori, T.; Saitoh, H.; Ikeda, T.; Aoki, K.; Fukui, H.; Funakoshi, K. *Phys. Rev. B* **2010**, *81*, 014109.
- (33) Braun, O. M.; Peyrard, M. *Phys. Rev. E* **2001**, *63*, 046110.
- (34) Braun, O. M.; Ferrando, R. *Phys. Rev. E* **2002**, *65*, 061107.
- (35) Mueser, M. H. *Phys. Rev. Lett.* **2002**, *89*, 224301.
- (36) Aichele, M.; Mueser, M. H. *Phys. Rev. E* **2003**, *68*, 016125.
- (37) Braun, O. M.; Manini, N. *Phys. Rev. E* **2011**, *83*, 021601.
- (38) Lemberg, H. L.; Stillinger, F. H. *J. Chem. Phys.* **1975**, *62*, 1677–1690.
- (39) Stillinger, F. H.; Rahman, A. *J. Chem. Phys.* **1978**, *68*, 666–670.
- (40) Duh, D.; Perera, D. N.; Haymet, A. D. J. *J. Chem. Phys.* **1995**, *102*, 3736–3746.
- (41) Yeh, I.-C.; Berkowitz, M. L. *J. Chem. Phys.* **1999**, *111*, 3155–3162.
- (42) Braun, O. *Surf. Sci.* **1989**, *213*, 336–358.
- (43) Koga, K.; Tanaka, H. *J. Chem. Phys.* **2005**, *122*, 104711.
- (44) Braun, O. M.; Paliy, M.; Consta, S. *Phys. Rev. Lett.* **2004**, *92*, 256103.
- (45) Jabbarzadeh, A.; Harrowell, P.; Tanner, R. I. *Phys. Rev. Lett.* **2005**, *94*, 126103.
- (46) Eisenberg, D.; Kauzmann, W. *The Structure and Properties of Water*; Oxford University Press: London, 1969.
- (47) David, C. W. J. *J. Chem. Phys.* **1996**, *104*, 7255–7260.
- (48) Braun, O. M.; Peyrard, M.; Bortolani, V.; Franchini, A.; Vanossi, A. *Phys. Rev. E* **2005**, *72*, 056116.
- (49) Braun, O.; Naumovets, A. *Surf. Sci. Rep.* **2006**, *60*, 79–158.
- (50) Braun, O. *Tribol. Lett.* **2010**, *39*, 283–293.
- (51) Lei, Y.; Leng, Y. *Phys. Rev. Lett.* **2011**, *107*, 147801.